Available online at www.sciencedirect.com
ScienceDirect
Journal of the European Ceramic Society 32 (2012) 85–95
www.elsevier.com/locate/jeurceramsoc

Controlled precipitation of W_2B_4 platelets and of β-WB nanolaminates for the *in situ* reinforcement of ternary TiB_2–W_2B_4–CrB_2 ceramics

Ai Momozawa, Rainer Telle *

RWTH Aachen University, Institute of Mineral Engineering (Gesteinshuettenkunde), Chair of Ceramics and Refractories (Lehrstuhl für Keramik und Feuerfeste Werkstoffe), Mauerstrasse 5, 52064 Aachen, Germany

Received 21 February 2011; received in revised form 14 July 2011; accepted 23 July 2011
Available online 19 August 2011

Abstract

Mechanical reinforcement of hard ultrahigh-temperature materials often requires complex processing techniques involving the mixing of platelet-shaped particles into the matrix – ultimately leading to inhomogeneities that compromise strength and fracture toughness. Thus, this paper investigates *in situ* reinforcement of a TiB_2 ceramic matrix by controlled precipitation of W_2B_4 platelets and β-WB nanolaminates. The results showed successful precipitation of: (i) W_2B_4 platelets according to the phase diagram, (ii) epitaxial β-WB lamellas, and (iii) spinodal, i.e. fully coherent W-rich lamellas which change to either W_2B_4 platelets or β-WB during ageing. The study of phase amount and microstructure as a function of homogenization temperature and annealing temperature/time regimes allows one to control the volume fraction, size as well as aspect ratio of precipitates. This enables the control of fracture toughness affected by crack deflection, particle pull-out, crack bridging and crack branching. Composition and milling treatment most affect microstructure. Successful precipitation is possible at 1650 °C.

Keywords: Borides; Composites; Platelets; Hot pressing; Inclusions

1. Introduction

TiB_2 and other transition metal diborides show outstanding thermomechanical and electrical properties making them prime candidates for very high temperature applications. Due to their strong covalent bonding in the boron sublattice, both the Young's modulus and hardness of diborides are so high that diborides have been considered as compounds in cutting tools or for ultrahigh-temperature structural applications. Their chemical stability and inertness make them suitable as crucible materials for melting metals or as thermocouple protection tubes for use in molten metals. Moreover, they display good electrical and thermal conductivities and corrosion resistance and are therefore attractive materials for cathodes or linings in aluminum reduction cells, heating elements[1] and evaporator boats for evaporation of metals in polymer tape-coating plants.[2] Besides ZrB_2, TiB_2 may also be considered as an ultrahigh-temperature material for thermal protection of re-entry space vehicles. For such applications, their poor sinterability, relative brittleness, and comparatively low strength should be overcome by second phase reinforcement as well as by an appropriate microstructural design.[3]

Many of the AlB_2-type transition metal diborides belonging to the space group *P6/mmm* exhibit a significant mutual solid solubility at high temperatures. Employing appropriate additives such as V, Cr, Mo, Hf, Ta, and partially also W that accommodate into this type of crystal lattice may generate accelerated volume diffusion and thus aid densification.

Telle et al. investigated the quasi-binary systems TiB_2–CrB_2, W_2B_4–CrB_2, and TiB_2–W_2B_4 and established the particular phase diagrams.[4] The combination of diboride solid solutions and W_2B_4 aimed at an *in situ* reinforcement of microstructures by forming a homogeneous $(Ti,W,Cr)B_2$ solid solution during a high-temperature treatment inside the widening single phase field. During cooling down into the two-phase region and annealing a second phase, in this case W_2B_4, was precipitated.[5] Since these precipitates usually possess a coefficient of thermal expansion different than that of the host crystal, intrinsic stresses are generated during final cooling. These stresses give rise to active crack deflection, microcracking, and load transfer[6]

* Corresponding author. Tel.: +49 241 8094968; fax: +49 241 8092226.
E-mail address: telle@ghi.rwth-aachen.de (R. Telle).

0955-2219/$ – see front matter © 2011 Elsevier Ltd. All rights reserved.
doi:10.1016/j.jeurceramsoc.2011.07.030

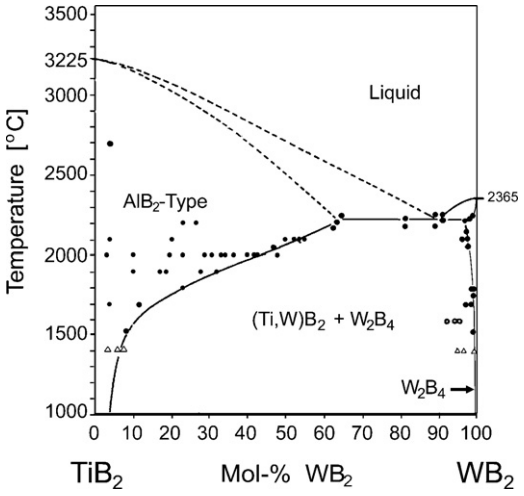

Fig. 1. Phase diagram of the TiB_2–WB_2. Black round dots refer to observed compositions of solid solutions. Triangular points are literature data.

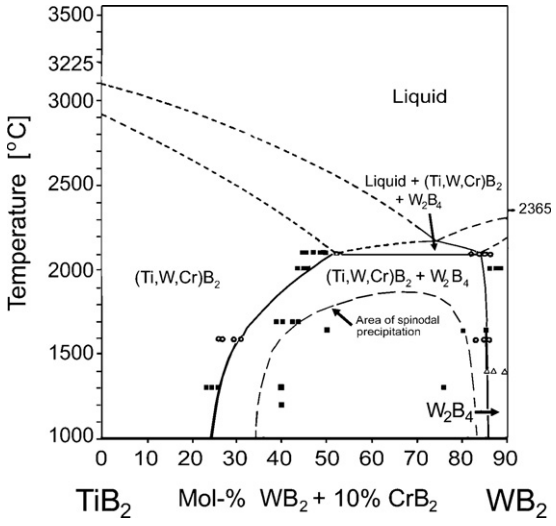

Fig. 2. Section through the TiB_2–WB_2–CrB_2 phase diagram parallel to the TiB_2–WB_2 edge at 10 mol% CrB_2. Black quadrangles refer to observed compositions of solid solutions.

in particular if the aspect ratio of the reinforcing phase is high.[7] Thus, the *in situ* growth of anisotropically elongated grains would be favored as this may overcome almost all problems involving homogeneous dispersion of powder particles of a high aspect ratio by mechanical methods as well as avoid differential shrinkage between matrix phase particles and the reinforcing phase during sintering.[8]

An interesting candidate for platelet-reinforcement is W_2B_4, space group $P6_3/mmc$, formerly denoted as W_2B_5.[9–11] This crystal structure consists of AlB_2-structure-type packages of different stacking sequences interrupted by puckered boron layers. Since it became experimentally evident that the theoretical stoichiometry of B/W = 2.5 is not fulfilled but approximates B/W = 2.0[11] this phase has been recently renamed. So as not to confuse it with the metastable AlB_2-type WB_2 as proposed by Woods et al.,[12] Frotscher et al. suggested the chemical formula W_2B_4 by referring to the different stacking modes but also accounting for the incomplete occupation of the boron sites.[13] Clarification of the true stoichiometry is, in fact, important, since most of the W_2B_4 powders commercially available are produced either by B- and W-powder solid-state reaction or by CVD processes typically erroneously using a stoichiometry of B/W = 2.5 for the initial components. Thus, these raw materials contain usually an excess of boron.

The TiB_2–W_2B_4 system is a eutectic system with the invariant point at 2230 ± 40 °C and 90 mol% W_2B_4 (Fig. 1). The solid solubility of W_2B_4 in TiB_2 at this temperature is approximately 63 mol%. The wide homogeneity range of the $(Ti,W)B_2$ solid solution narrows significantly with decreasing temperature. At 2000 °C, the maximum solubility ranges between 44 and 46 mol% W_2B_4, and at 1500 °C it is 7–8 mol%, while the TiB_2 content in W_2B_4 is reduced from 3 to 4 mol% to 2 and <1 mol%, respectively.

Mitra and Telle[14] established a section of the quasi-ternary phase diagram of the TiB_2–W_2B_4–10 mol% CrB_2 system (Fig. 2) in order to enhance volume diffusion by adding CrB_2 and to reduce temperature and time for the annealing treatment, while another goal was to influence thermal expansion coefficients.[15] With the addition of CrB_2, the maximum solubility of W_2B_4 in AlB_2 structure phase decreased from 63 mol% to 58 mol%, but the three-phase equilibrium comprising a liquid was shifted to 1980–2000 °C. Consequently, the homogeneity range in the experimentally more accessible region below 2000 °C was extended.

The aim of this present study is to systematically investigate the ternary TiB_2–W_2B_4–CrB_2 compositions with special focus on 40 mol% TiB_2, 50 mol% W_2B_4, and 10 mol% CrB_2 in order to determine the precipitation mechanisms and kinetics more precisely and to establish suitable temperature–time regimes for generating *in situ* platelet-reinforced microstructures.

2. Materials and methods

The starting powders made up of TiB_2, W_2B_4 and CrB_2 were supplied by Japan New Metals Co., Ltd., Osaka, Japan, and Hermann C. Starck GmbH, Goslar, Germany. Their characteristics are shown in Table 1. The particle size distribution was determined by laser-scattering (Mastersizer 2000, Malvern Instruments, UK). The boron content of powders was measured by ICP (PerkinElmer Plasma 2000) after acidic leaching. Both powders differed with respect to TiB_2 grain size and contaminants. The W_2B_4 powder from Japan New Metal showed a nominal B/W ratio of 2.6, whereas that from the H.C. Starck company had a nominal B/W ratio of 2.4. It should be noted, however, that the major impurities carbon and nitrogen are bonded as B_4C, and BN, respectively, while excess B may be present as B_2O_3.

The powders were mixed in different molar ratios ranging from $65TiB_2$–$15W_2B_4$ to $10TiB_2$–$80W_2B_4$ while the CrB_2 content was fixed at 10 mol%. The H.C. Starck powder was predominantly used for precipitation studies. In this paper, most results will reflect a TiB_2:W_2B_4:CrB_2 composition of 40:50:10 mol%. The pre-mixed powders were attrition-milled in a 500 ml stainless steel container (stirrer rotor and excenter

Table 1
Chemical composition of starting powders (wt.%).

	Size (μm)	Ti	W	Cr	B	C	N	O	Fe
(a) Japan New Metal Co., Ltd., Osaka, Japan									
TiB_2	4.25	68.17	–	–	30.59	0.22	0.64	0.29	0.09
W_2B_4[a]	2.50	–	85.91		13.13	0.68	0.24	0.04	0.00
CrB_2	5.40	–	–	69.46	29.81	0.11	0.40	0.22	0.00
(b) H.C. Starck GmbH, Goslar, Germany									
TiB_2	25.0	68.62	–	–	30.77	0.25	0.04	0.17	0.15
W_2B_4[a]	2.2	–	87.03	–	12.39	0.29	0.00	0.19	0.10
CrB_2	4.3	–	–	70.29	29.20	0.21	0.00	0.18	0.12

[a] Commercially available as W_2B_5.

disks armored by WC/Co) together with 1 mm diameter WC/Co balls (Netzsch-Feinmahltechnik, Selb, Germany, 94 wt.% WC, 6 wt.% Co) in isopropanol at 1000 min^{-1} for 2 h. After milling, the suspension was dried and granulated in a rotary evaporator.

The powder was hot-pressed (F 8127 HPW200/250-2200-18KS, FCT, Rauenstein, Germany) in hexagonal boron nitride-lined graphite dies with graphite resistance heating and homogenized at temperatures of 2000 °C and 2100 °C in 1 atm of Ar atmosphere, under a pressure of 50 MPa for holding times of between 0.5 h and 14 h, respectively. A heating rate of 20 K/min from room temperature to 1200 °C was followed by increments of 10 K/min until the temperature limit was reached. The hot-pressed samples were subsequently cooled down under pressure release to temperatures of 1500, 1600, 1650, and 1700 °C and annealed for phase separation for various durations from 0.5 h to 16 h, respectively. The final cooling rate was 20 K/min to 1100 °C followed by free cooling to room temperature. The temperature was controlled by a Pt5%Rh–Pt20%Rh thermocouple and an optical pyrometer above 1200 °C that was calibrated by a Planckian black emitter.

Microstructural characterization and local elemental analysis were performed on diamond-ground and polished samples with a scanning electron microscope (SEM, Leo 440i, Leo Electron Microscopy, Cambridge, UK) and energy dispersive X-ray spectroscopy (EDS, Oxford EDX, system Link Isis). Transmission electron microscopy was carried out with a CM30 at 300 kV acceleration voltage (Philips, Eindhoven, The Netherlands) and a CM300UT-FEG (Philips) equipped with an electron energy loss spectrometer (EELS) for light element detection. Additionally, microprobe analysis for boron was conducted with a JEOL JXA-8600 Superprobe. The respective phase content of both polished sections as well as of powderized hot-pressed and temperature-treated samples was measured by X-ray diffraction (XRD) analysis using a Philips diffractometer (PW3710, Philips, Eindhoven) with CuK_α radiation.

3. Results

3.1. Reactions of starting materials

Heating up the powder bodies of the various mixes resulted in an increasing interdiffusion among TiB_2, W_2B_4, and CrB_2. Generally, the CrB_2 phase dissolved very fast into $(Ti,Cr)B_2$ and $(W,Cr)_2B_4$ so that at 1400 °C and above no distinct CrB_2 phase could be detected anymore. A high CrB_2-content enhanced the W dissolution in $(Ti,W,Cr)B_2$.

Fig. 3 shows a SEM micrograph with a non-equilibrium situation of W_2B_4-consumption (light grain) by the two neighboring $(Ti,W,Cr)B_2$ particles. Note that no CrB_2 is visible but that two rim areas of increasing W- and Cr-content are seen around the initial center points of former TiB_2 particles. The black particles in the center and at the lower border are either hexagonal BN or graphite as multiply proven by XRD (best fit by cliftonite reflections) and TEM combined with EELS.[5] Traces of $(W,Ti)C_{1-x}$ can rarely be found by XRD at temperatures up to 1650 °C.

Homogenization of the TiB_2:W_2B_4:CrB_2 = 40:50:10 mol% composition at 2000 °C is incomplete even after 12 h. Although this composition is close to the maximum W-solubility but still inside the single phase field, residual undissolved W_2B_4 phase, elemental boron or carbon and – in rare cases – $(Ti,W,Cr)B_2$ grains with cores of unreacted TiB_2 are found. Almost all of the initial phases reacted to a homogeneous solid solution after heating to 2100 °C for 6 h. The average grain size ranges now between 50 and 80 μm. Fine grains of graphite, and, in the case of a high W_2B_4 content, boron were predominantly arranged at the grain boundaries. There was no difference in grain size or phase composition if comparing the as-homogenized microstructures prepared from H.C. Starck and Japan New Metals powders.

Homogenization at 2100 °C for 6 h starting from a TiB_2:W_2B_4:CrB_2 molar composition of 65:25:10 with stepwise increments of 10 mol% W_2B_4 to the W-rich end com-

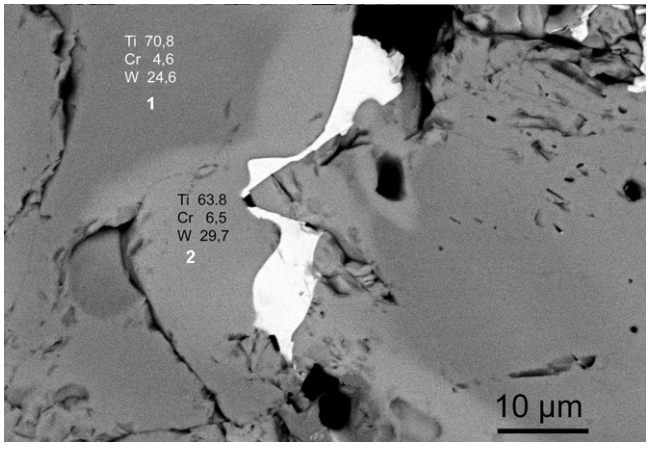

Fig. 3. W_2B_4 dissolution during heating (light phase); compositions in mol%.

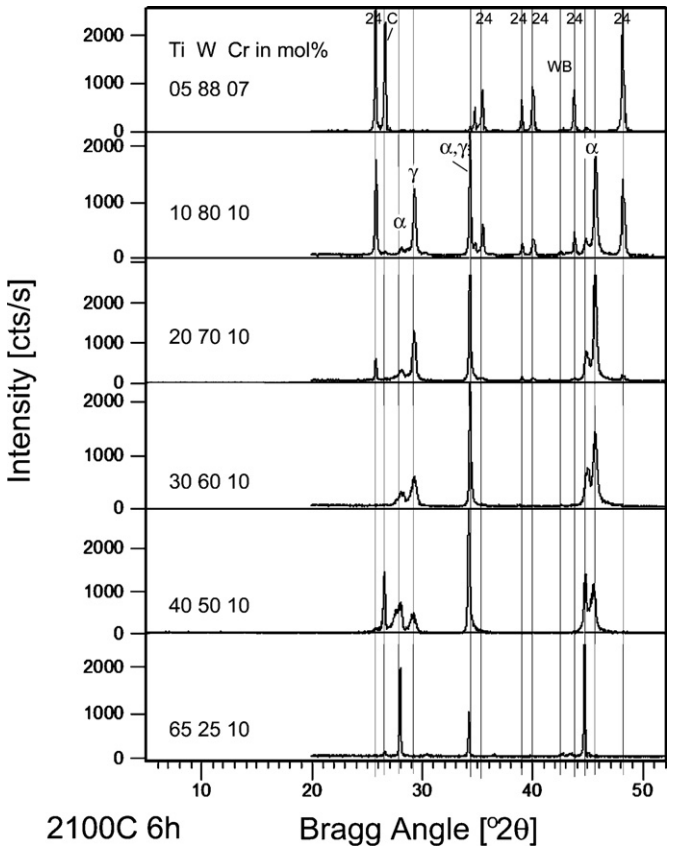

Fig. 4. X-ray diffraction pattern of samples with varying Ti:W ratio annealed at 2100 °C for 6 h. α and γ refer to two kinds of *P6/mmm*-structure type (Ti,W,Cr)B_2 solid solutions. "24" refers to W_2B_4, C is graphite, WB is β-WB. Note 0 0 2 peak splitting between 28° 2θ (α-phase) and 29° 2θ (γ-phase) while 1 0 0 reflection at 34.1° 2θ is not significantly affected.

position of 05:88:07 reveals that the composition of the $(Ti_{0.9-x},W_x,Cr_{0.1})B_2$ increases continuously until the maximum solubility of W_2B_4 is reached at $(Ti_{0.41},W_{0.49},Cr_{0.1})B_2$ and the two-phase-equilibrium is entered. At compositions of 10:80:10 and higher W_2B_4-content, an unexpected third phase, β-WB, appears and disappears again upon approaching a TiB_2 content of <5 mol%. Moreover, XRD diagrams reveal a peak-splitting of 0 0 l-reflections pattern of (Ti,W,Cr)B_2. Starting with a single phase composition in case of a Ti:W:Cr ratio of 65:25:10, denoted as α in Fig. 4, a second broader 0 0 1-peak of another kind of (Ti,W,Cr)B_2, here denoted as γ, is steadily increasing at the expenses of the 0 0 2-peak of α while increasing the W-content. The α-phase, however, exhibits a slight lattice contraction with increasing W-content, too. Both solid solutions belong to the *P6/mmm*-type but vary in regard to the lattice constant c_o as can be seen from the coincidence of 1 0 0 reflection at 34.1° 2θ. Both phases disappear entirely at a W_2B_4-concentration exceeding 85 mol%. Note also the existence of clear graphite reflections at diffraction angles of 26.4° 2θ. There is also evidence for formation of a local liquid phase at triple points and in the vicinity of pores. EDS area analysis of solidified liquid shows 31 mol% Ti, 13 mol% Cr, and 56 mol% W.

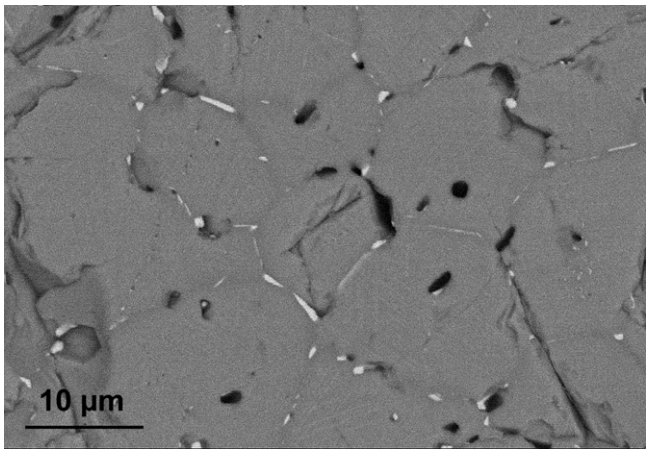

Fig. 5. Initial state of heterogeneous nucleation of W_2B_4 (light) at grain boundaries.

3.2. Precipitation reactions

Since hot pressing at 2000 °C for 4 h was suitable enough for densifying and avoiding CrB_2 evaporation we choose a 4 h pressureless post-treatment at 2100 °C for final homogenization, followed by precipitation annealing at lower temperatures. Shorter homogenization time leave relatively small residual particles of starting W_2B_4 powder behind at the grain boundaries of the saturated solid solutions.

3.2.1. Formation of W_2B_4 platelets

Precipitation of W_2B_4 starts by heterogeneous nucleation at grain boundaries between the supersaturated (Ti,W,Cr)B_2 solid solution as identified by XRD and selected area electron diffraction in the TEM. Typical platelet-shaped crystals grow along the grain boundary or into the neighboring particles while crossing the grain boundaries (Figs. 5 and 6). If residual undissolved W_2B_4 is present, these particles act as nucleation sites during cooling, too. Starting preferentially at the phase boundaries of these grains, the platelets expand into the surrounding solid solutions. Thus, the initially round and equiaxed particles become blocky and elongated with smooth crystal faces some-

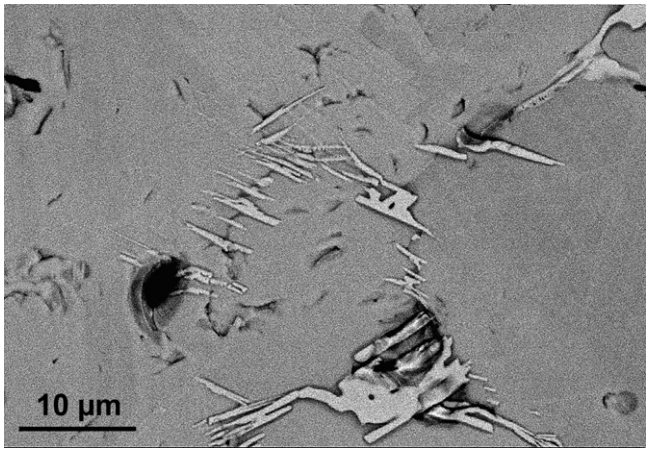

Fig. 6. Progressed growth of W_2B_4 (light) across grain boundaries.

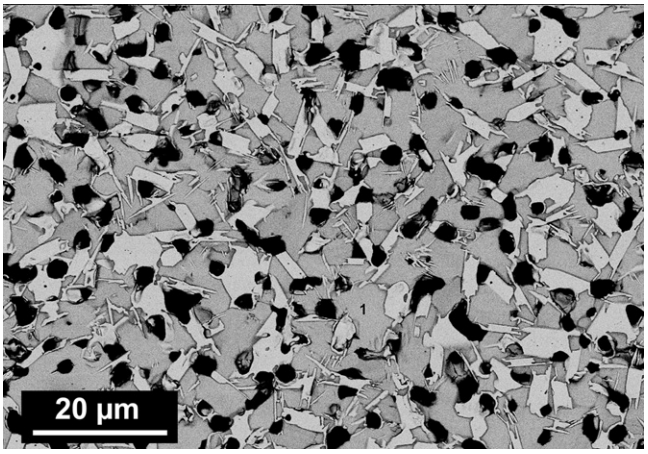

Fig. 7. Growth of undissolved W_2B_4 residues (light) during cooling and further annealing.

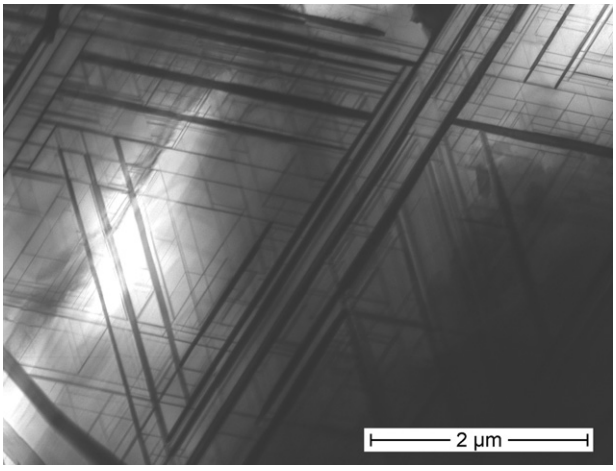

Fig. 9. TEM image of epitaxial β-(W,Ti,Cr)B precipitates in (Ti,W,Cr)B_2 host crystal.

times having platelets attached (Fig. 7). Both precipitates contain a molar fraction of 4–6 mol% TiB_2 and up to 7 mol% CrB_2. The lattice parameters of (W,Cr,Ti)$_2B_4$ are $a_o = 0.2978(2)$ nm and $c_o = 1.385(1)$ nm as measured by both HR-TEM and selected area electron diffraction.

3.2.2. *Formation of β-WB epitaxial precipitates*

According to the expectations from the phase diagram, W_2B_4 should solely be precipitated. Another kind of precipitation, however, is generated by nucleation inside the supersaturated (Ti,W,Cr)B_2 host crystal and epitaxial intergrowth. Both XRD and HR-TEM together with electron diffraction prove this phase to be β-WB (orthorhombic, *Cmcm*). β-WB forms very thin platelets and is crystallographically well orientated in three directions intersecting at an angle of 120°, i.e. parallel to the prism planes of the hexagonal host crystal, $\langle 1\,\bar{1}\,0\,0\rangle_{(Ti,W,Cr)B_2} \| (0\,1\,0)_{\beta-WB}$ and $[0\,0\,0\,1]_{(Ti,W,Cr)B_2} \| [1\,0\,0]_{\beta-WB}$ (Figs. 8–10). According to EELS-analysis,[5] the high-temperature form β-WB is stabilized by accommodation of up to 50 at.% Ti and 20 at.% Cr and should therefore be denoted as β-(W,Ti,Cr)B. Both stabilization and epitaxial growth is made possible by a very small lattice expansion resulting in a perfect fit to the lateral dimensions of the $\langle 1\,\bar{1}\,0\,0\rangle$ plane of the (Ti,W,Cr)B_2 host crystal. The mismatch between the atomic site positions of both planes as estimated by HR-TEM is approximately 1%. A typical well-accommodating situation is the neighborhood of $(Ti_{0.55}W_{0.32}Cr_{0.12})B_2$ and β-$(W_{0.44}Ti_{0.44}Cr_{0.12})$B. Observations by SEM and HR-TEM reveal that the monoboride platelets are 0.8–10 nm thick and consist of 1–12 unit cells only, whereas the lateral extension is limited by the size of the host crystal and may approach several 100 μm.

Another type of β-(W,Ti,Cr)B is observed as particle clusters which may be considered as undissolved residues from the starting W_2B_4 material including WC debris from the milling process. These aggregates extend for 20–50 μm and consist of homogeneous β-monoboride surrounded by clusters of graphite. During annealing at lower temperatures, slightly darker inclusions of blocky fan-like arranged platelets of (W,Ti,Cr)$_2B_4$ grow from the interface to the environmental matrix either into the clusters or expanding to the outside (Fig. 11). The

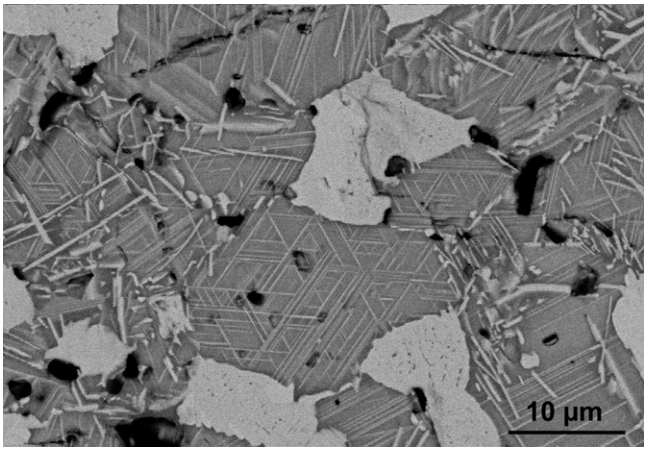

Fig. 8. Epitaxial β-(W,Ti,Cr)B precipitates as seen parallel to [0 0 0 1] (center) between clusters of β-WB/W_2B_4.

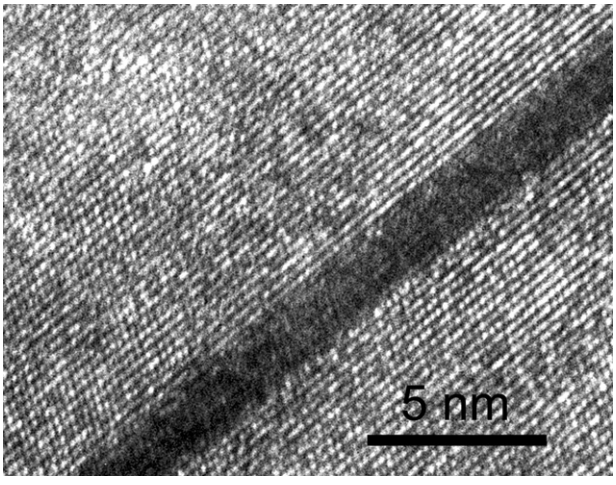

Fig. 10. HR-TEM micrograph of β-(W,Ti,Cr)B coherently bonded to (Ti,W,Cr)B_2 host crystal.

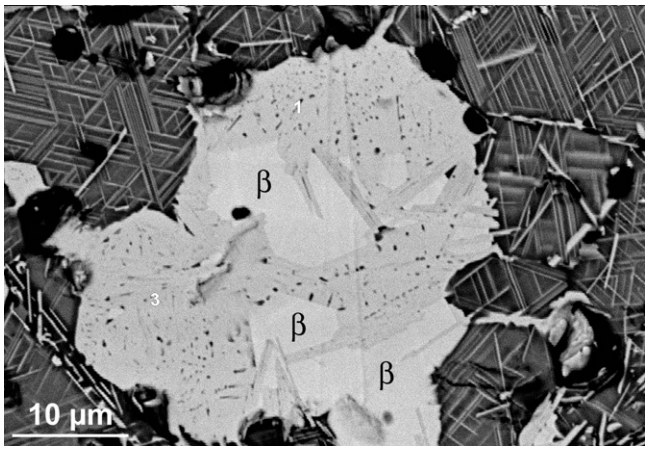

Fig. 11. Cluster of W-rich compounds, hot-pressed at 2000 °C for 8 h, annealed at 1500 °C for 8 h. Note the growth of W_2B_4 inside β-WB and epitaxial β-WB precipitates in the surrounding matrix. Black flakes are graphite, black dots inside W_2B_4 aggregates are pores.

β-(W,Ti,Cr)B solid solution can be recognized by its brighter atomic number contrast due to the lower boron content. As determined by high resolution microprobe analyses, the composition is: W = 46.5 at.%, Ti = 2.5 at.%, Cr = 0.1 at.%, B = 50.9 at.% yielding an atomic (W + Ti + Cr):B ratio of 1:1.04. The intergrowths of $(W,Ti,Cr)_2B_4$ show a composition of W = 33.0 at.%, Ti = 1.8 at.%, Cr = 0.05 at.%, B = 65.1 at.% and a (W + Ti + Cr)-to-B ratio of 1:1.87 which is typical for this phase.[11]

3.2.3. Formation of spinodal precipitates

Spinodal decomposition of the supersaturated $(Ti,W,Cr)B_2$ solid solution is also observed. The typical wavy and diffuse outline of the precipitates without sharp interfaces to the host crystal is shown in Fig. 12. HR-TEM micrographs prove their atomistic three-dimensional fit to the host lattice. Sometimes the precipitates are aligned in a parallel mode and may split up into

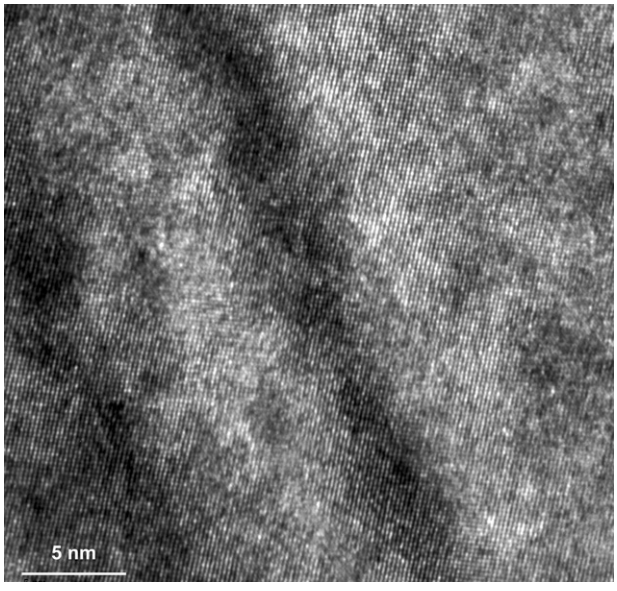

Fig. 12. HR-TEM micrograph of W-rich area (dark). Note smooth contrast undulation between precipitate and host crystal.

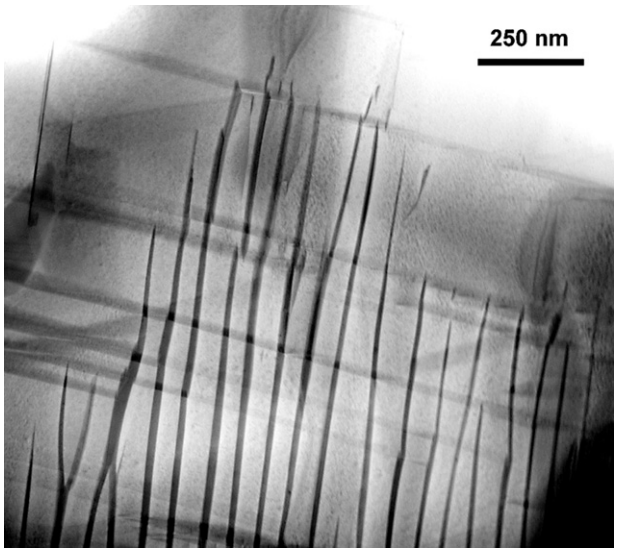

Fig. 13. TEM micrograph of intersection of spinodal (vertical) and epitaxial precipitates (horizontal). Note the interruption and stop of spinodal precipitates while meeting epitaxial precipitates.

two or more branches (Fig. 13). The light contrast in SEM and the dark one in TEM indicate that this area is enriched in tungsten. Convergent beam electron scattering studies reveal that these areas belong to the same space group *P6/mmm* and pointgroup *6mm* as the host crystal and obey the same rules of extinction. Therefore, any ordering of W-atoms on Ti-sites can be excluded. However, the lattice constant of the precipitates $c_o = 0.310(5)$ nm is slightly smaller than $c_o = 0.322(5)$ of the host crystal which seems to be the only influence of the enrichment in tungsten.

Depending on the local concentration of Ti, W, and Cr, as well as on the thermal history, the precipitates become unstable and differentiate from AlB_2-type into either W_2B_4 or β-(W,Ti,Cr)B during ageing. This development is controlled by both chromium and boron diffusion. Depletion in boron at a relatively high chromium level means ageing to β-(W,Ti,Cr)B platelets while depletion in chromium at a metal-to-boron ratio of around 1:2 results in W_2B_4 formation (Fig. 14). Regarding the sequence of precipitation, there is evidence that spinodal decomposition follows shortly after epitaxial precipitation, since the spinodal precipitates sometimes stop or even bend or split at the β-(W,Ti,Cr)B-lamellas (Fig. 13).

3.2.4. Behavior of $(Ti,W,Cr)B_2$ solid solution during precipitation

Fig. 15 shows a time-dependent XRD-diagram compilation of a 40 mol% TiB_2, 50 mol% W_2B_4, and 10 mol% CrB_2 composition hot-pressed at 2000 °C for 8 h followed by annealing at 1700 °C for 0–8 h. Cooling down immediately after homogenization ("0 h") already reveals the two types of $(Ti,W,Cr)B_2$ solid solutions with *P6/mmm* structure, α and γ, which can be identified by the 0 0 1 reflections. The 0 0 1-peak of γ is rather weak in intensity but very broad while the pattern of α is very close to that of TiB_2 taking Vegard's rule of mixture into account. A higher resolution of this XRD diagram shows, however, that $(W,Ti,Cr)_2B_4$, β-(W,Ti,Cr)B, and residual $(W,Ti)C_{1-x}$

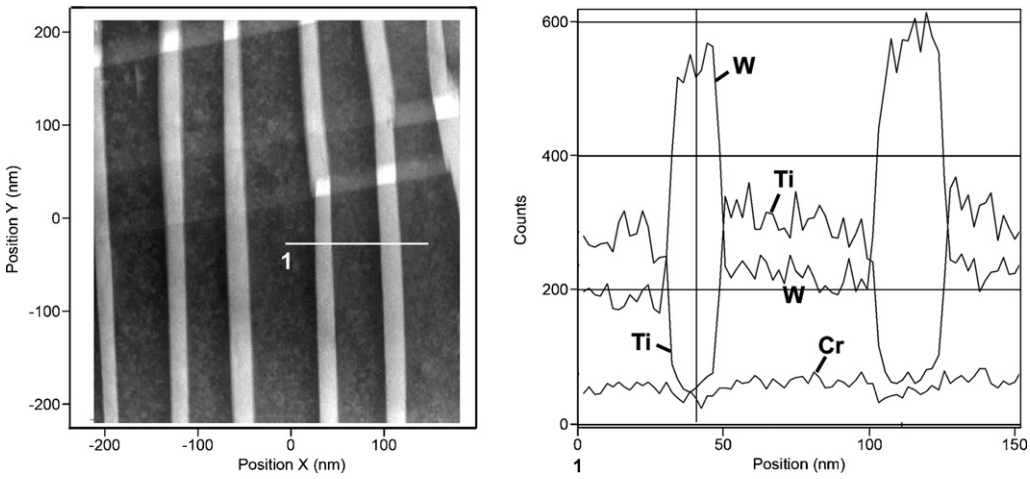

Fig. 14. Spinodal precipitates aged to W_2B_4 structure. TEM-EDS linescan reveals a sharp gradient in W and Ti while Cr is almost not affected.

are present in very small concentration, too. During annealing at lower temperature the 0 0 l reflections of the γ are reduced in intensity and vanish after annealing at 1700 °C for 4 h most likely to the benefit of the growing β-(W,Ti,Cr)B phase as indicated by its sudden increase in intensity. Simultaneously – at most, however, after γ decomposed entirely – supersaturated α releases tungsten for the growth of W_2B_4, i.e. at 1700 °C from 2 h annealing time on. Another source of tungsten is the chemically instable WC_{1-x} from the debris of the milling balls which decompose into graphite while releasing W. Surprisingly, no boron carbide has been found in all cases.

Due to the precipitation of W-rich phases, the α-(Ti,W,Cr)B_2 becomes locally W-depleted. This can be observed in the SEM by the change in atomic number contrast. In particular in case of spinodal decomposition the host crystal releases significantly more W compared to the epitaxial precipitation. The residual W-content varies between 30 and 33 mol% whereas particles with >45 mol% W are metastable or undergo phase separation.

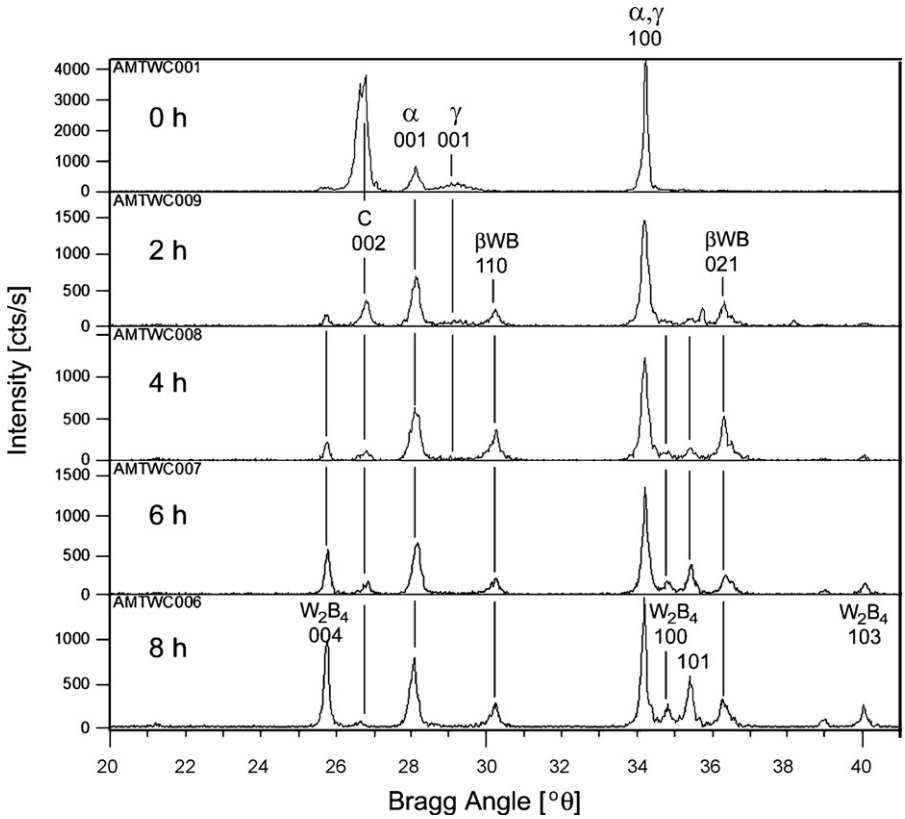

Fig. 15. Compilation of XRD pattern for a 40 mol% TiB_2, 50 mol% W_2B_4, and 10 mol% CrB_2 composition as hot pressed at 2000 °C 8 h ("0 h") and subsequently annealed at 1700 °C for 2–8 h. Note the broad 0 0 2 peak of γ and the increase in both W_2B_4 and β-WB intensity. C refers to graphite.

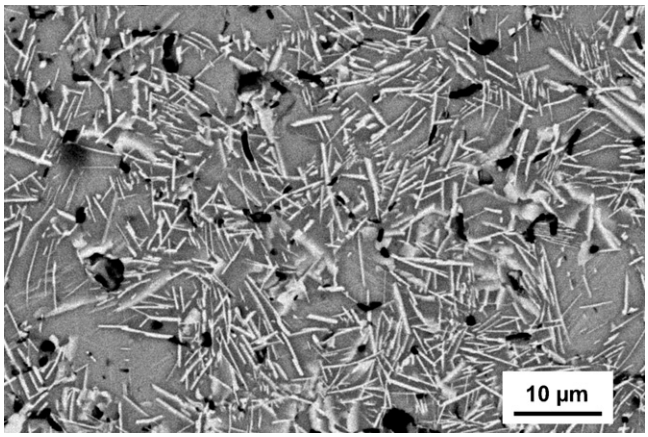

Fig. 16. Typical microstructure after annealing at 1650 °C 4 h.

3.2.5. Final microstructure after annealing at lower temperatures

Since all precipitation reactions run almost simultaneously, the resulting microstructure becomes rather complex (Fig. 16). There are large areas belonging to the former solid solutions now exhibiting both epitaxial and spinodal precipitates that look like cells interlocked by a network of thin platelets. More or less isolated equiaxial clusters of tungsten-rich phases exist, grown from residual W_2B_4-particles, internally consisting of blocky β-(W,Ti,Cr)B- and $(W,Ti,Cr)_2B_4$-platelets. There are also very small graphite inclusions which are sometimes interconnected to hexagonal boron nitride and probably also to boron suboxides. Some residual porosity of <1–2% can be attributed to the evaporation of Cr–Co–B-alloys and CrB_2, lack in densification and pull-out of particles during grinding and polishing of the samples. Since the volume fraction of platelets depends on starting composition and both size and aspect ratio on the thermal treatment, it is obvious that there are many options to influence the microstructure for further optimization in respect to mechanical properties (Fig. 17).

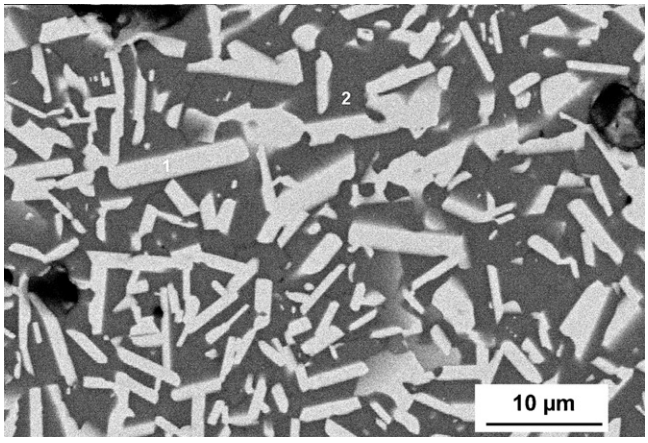

Fig. 17. Coarsened $(W,Cr,Ti)_2B_4$ platelets in $(Ti,W,Cr)B_2$ matrix.

4. Discussion

4.1. Influence of mixture composition

The development of the microstructures of different TiB_2/W_2B_4 mixture ratios in the TiB_2–W_2B_4–CrB_2 system was investigated, while the CrB_2 amount was kept constant at 10 mol%. Hot pressing at 2100 °C results in homogeneous $(Ti,W,Cr)B_2$ solid solutions if the W_2B_4 concentration does not exceed 45 mol%. These phases do not change if annealed at lower temperatures. No W_2B_4- or β-WB-type precipitates grow even after treatment at 1300 °C for 8 h. These compositions are located in a single phase field of the pseudo-ternary system, accordingly.

Compositions with a W_2B_4 concentration of between 40 mol% and 45 mol% result in $(Ti,W,Cr)B_2$ solid solutions if treated at 2100 °C, but clusters of undissolved W_2B_4/β-WB are present when sintered at 2000 °C. This is attributed to the temperature-dependent saturation limit of tungsten in $(Ti,W,Cr)B_2$.

Formation of β-WB from W_2B_4 was described by Kuzenkova et al.[16] who observed the decomposition of W_2B_4 into 2 WB + 2 B during heating up to temperatures of >1600 °C and who argued that WB is the more stable phase. According to the most recent phase diagrams,[17,18] however, this is not very likely under equilibrium conditions, as the homogeneity range of W_2B_4 becomes slightly larger with increasing temperature. Nonetheless, evaporation of boron compounds such as boron suboxides may also shift the overall composition to boron deficiency. Thus, Kuzenkova's β-WB formation may be explained by internal oxidation of B by CO, thereby generating boron oxide. It should be emphasized, however, that WC from the milling balls is present in our system, which may react with W_2B_4 during heating, first, according to $2WC + W_2B_4 \rightarrow 4WB + 2C$, and, in a second step during cooling, according to $2WB + 2B \rightarrow W_2B_4$. The source of free boron supply for this reaction may be then found in the epitaxial precipitation of β-(W,Ti,Cr)B inside the supersaturated $(Ti,W,Cr)B_2$ solid solutions close to the W_xB_y-clusters (Fig. 6). The clearly visible porosity trapped inside W_2B_4 is a consequence of its lower specific volume. Missing transformation from β-(W,Ti,Cr)B to α-(W,Ti,Cr)B below 2170 °C[17] is explained[16] by the presence of carbon (sintering of W_2B_4 in a C/CO/Ar atmosphere). Moreover, some transition metals such as Ti, Zr, and Hf are known to stabilize the high-temperature modifications of both WB and isotypic MoB at lower temperatures.[19] In fact, the authors report the incipient formation of α-WB after annealing at temperatures of 1700 °C and lower.

A W_2B_4 content exceeding 55 mol% gives rise for the formation of γ-type $(Ti,W,Cr)B_2$ with $c_o/a_o = 1.01–1.02$. Broadening of 0 0 l reflections is attributed to planar lattice defects in the basal plane of the crystal with a wide and smooth distribution of local c_o values ranging from $d_{0\,0\,l} = 0.303$ to 0.307 nm while the d_{hk0} are very close to those of α which makes lattice parameter refinement difficult. Using the c_o/a_o ratio as a criterion for distinction to α with $c_o/a_o = 1.05–1.06$, γ clearly deviates with $c_o/a_o = 1.01–1.02$ and is more similar to the *P*6/*mmm*-type MoB_2 with $c_o/a_o = 1.01–1.02$, CrB_2 with $c_o/a_o = 1.02–1.03$, and WB_2

with $c_o/a_o = 1.01$[12] which opens again speculation whether the latter phase is stabile or not.

At W_2B_4 concentrations of >65 mol%, partial melting is locally observed, in particular, where initial CrB_2 particles have formerly been in contact with W_2B_4 grains. At 2100 °C from 85 mol% W_2B_4 on upwards the two phase field $(W,Cr,Ti)_2B_4$-liquid is entered. The microstructure of these very W_2B_4 rich compositions will be subject for another publication.

Upon comparing the microstructures of samples after homogenization that are annealed at temperatures of <2000 °C, compositions of between 30 mol% and 90 mol% W_2B_4 – depending on the temperature – show extensive *in situ* growth of $(W,Cr,Ti)_2B_4$ or epitaxial β-(W,Cr,Ti)B. Within smaller margins between 40 and 80 mol%, W_2B_4 spinodal precipitates are generated. These local undulations in W-concentration mature through transformation into either $(W,Cr,Ti)_2B_4$ or β-(W,Cr,Ti)B depending on the local boron and chromium availability.

4.2. Role of CrB_2

In general, CrB_2 is neither required to form $(Ti,W)B_2$-type solid solutions nor to facilitate $(W,Ti)_2B_4$ precipitation. However, CrB_2 accelerates phase formation clearly by enhancing the volume diffusion. Schmidt et al.[20] studied ^{49}Ti and ^{54}Cr tracer diffusion in $(Ti_{0.3}W_{0.5}Cr_{0.2})B_2$ ceramics at temperatures ranging from 1100 °C to 1400 °C. They proved a diffusion coefficient that was one order of magnitude greater for Cr than for Ti. This is experimentally confirmed by many hot-pressing treatments with and without the aid of CrB_2. Unfortunately, a high CrB_2 content also bears the risk of evaporation during heat treatment at temperatures of >1900 °C, thus leaving pores behind.

There are obviously three options for melting in the TiB_2–WB_2–10 mol% CrB_2 system studied: first of all, there is a risk of running the hot press temporarily at slightly higher temperatures than the 2100 °C scheduled, in particular during heating up the system. Secondly, if the local concentration of CrB_2 (T_m = 2157–2200 °C) is high enough, e.g. due to CrB_2 agglomerates, the composition of this area could be located in the binary liquid–W_2B_4 equilibrium or in the ternary liquid–$(Ti,W,Cr)B_2$–W_2B_4 equilibrium the borders of which are still not explored yet. Since the overall microstructure does not exhibit the typical features of liquid phase sintering it is concluded that this liquid is transient since all compounds will diffuse out into the surrounding solid solutions. The third case of liquid phase formation may occur if the W_2B_4 concentration exceeds 85 mol% while the local CrB_2 content is >8–10 mol%.

4.3. Role of carbon

Most of the black contrasts observed in SEM images are graphite or pores (Figs. 6 and 11). Carbon mainly originates from the wear debris from WC/Co balls by attrition milling but also from the graphite crucible. There is some carbon in the starting powders, too (Table 1). After 2 h of milling, the weight gain is 5–12% depending on the volume fraction of the most abrasive compound TiB_2. Under the present experimental conditions, WC starts to decompose at 2000 °C and is not detectable anymore by XRD or SEM after hot-pressing at 2100 °C. It seems that carbon does not react with any other species, whereas tungsten reacts with boron provided by W_2B_4, and primarily forms β-(W,Ti,Cr)B. Carbon just coagulates as graphite at the grain boundaries or at the triple points of the matrix particles. It cannot be empirically excluded that some carbon replaces boron in the boride structure by sp^2 hybridization, too. Rogl gives a maximum C-solubility of 3.2 at.% in W_2B_4 and of 0.6 at.% in β-WB at 2167 °C and of 2.5 at.% upon transformation to α-WB at 2149 °C.[19] Contrary, Aronson et al. argue that C → B substitution in metal borides is not very likely because of the small B-B distances. It is only expected in NaCl- and WC-structure type phases such as RuB, they proposed.[21] Their studies in the W_2B_4–WC system obviously did not yield any evidence of substitution. Since solid solutions and planar defects play a major role in our results we would not like to entirely exclude a C → B replacement. Besides this, there is also a beneficial role of C, namely to remove oxygen contamination from the boride powders. Since this will happen during heating-up the green-bodies, it is most likely that also the initial C-content of the raw materials (Table 1) is used up by this reaction. Regarding mechanical properties, both the concentration and grain size of free carbon should be minimized. Free carbon located at the grain boundaries could also positively affect fracture toughness. Sigl and Kleebe[22] prepared B_4C–TiB_2 composites from B_4C + TiC powder mixes, thereby yielding very thin graphite lamellas at the phase boundaries which caused enhanced crack deflection.

4.4. Influence of Co contamination

The role of Co in the system is not yet readily understood. A wet chemical analysis of a TiB_2:W_2B_4:CrB_2 = 40:50:10 mol% starting powder blend yielded 0.4–0.5 wt.% Co content after 2 h of attrition-milling. From other studies of attrition-milled B_4C–TiB_2–W_2B_4 samples, it is known that Co reacts with boron, thereby creating a liquid phase in the temperature range of 1100–1300 °C.[23] This liquid tends to evaporate at higher temperatures in a vacuum. This is most likely in our system, too. Co is rarely observed together with W, Ti, Cr and B at triple points after the homogenization treatment. Co may also enhance particle rearrangement and aid densification by grain growth with transient liquid phase. This mechanism varies to that proposed by Sibuya et al.[24,25] who prepared $(Ti,W)B_2$ solid solutions by field-activated combustion sintering with 0.5–1.0 wt.% Co and Ni, respectively, and subsequently annealed the samples in the two phase region TiB_2–W_2B_4. They hereby suppose that both metals might enhance the decomposition of the supersaturated solid solution. However, it is to be noted here that in our EDS studies using SEM and TEM, Co was never found inside or around precipitates but, if at all, at triple points or inside pores filled with consolidated liquid phase.

4.5. Process control

Since an ultimate goal is to tailor specific microstructures that satisfy mechanical requirements, the investigation of the phase formation mechanism shows some key parameters for obtaining both high fracture strength and toughness. Thus, a composition regime revealing microstructures with well-dispersed W_2B_4 precipitates has been identified. The experimental results support the expectation that an attrition-milled mixture consisting of 40 mol% TiB_2, 50 mol% W_2B_4 and 10 mol% CrB_2 is an excellent candidate for improving mechanical properties. Randomly oriented W_2B_4 precipitates may contribute towards increasing fracture toughness. As the B-content determines the amount of W_2B_4 and β-WB, the use of H.C. Starck powder favors W_2B_4 precipitation due to its surplus of boron. However, mixtures from Japan New Metals powder generate more β-WB due to the slight boron deficiency. One can control the B/W ratio by adding extra B or metal powder, respectively. It is expected that boron in excess reacts with carbon to yield boron carbide. By contrast, boron is preferentially accommodated in the next higher boride structures due to their higher enthalpy of formation.

As noted above, a small amount addition of CrB_2 accelerates densification and homogenization, but may cause pores by evaporation. Thus, hot-pressing at 2100 °C for long times should be avoided and field-activated combustion synthesis used instead[8] – a treatment which was not available here.

5. Conclusion

The huge range of solid solubility of transition metal diborides in the pseudoternary system TiB_2–CrB_2–W_2B_4 at temperatures exceeding 2000 °C allows for a homogenization treatment followed by controlled undercooling to temperatures at which phase separation is initiated by prolonged annealing. Both *in situ* growth of residual undissolved particles as well as epitaxial or spinodal precipitation of second phases such as Ti- and Cr-bearing solid solutions of W_2B_4 and β-WB can be initiated in order to create microstructures tailored for an *in situ* particle reinforcement. Limiting this study to a TiB_2–W_2B_4 series with a CrB_2 content of constant 10 mol% shows that homogenization is completed by hot-pressing at 2100 °C for 4–8 h. Treatment at lower temperature or for a shorter time leaves residual particles or particle cores unreacted behind which may act as nuclei for heterogeneous precipitation upon annealing at lower temperatures.

Epitaxial precipitation of a β-WB-structure type phase is enabled by accommodating both Ti and Cr and, thus, by expanding the crystal lattice until it perfectly fits to the host crystal. These monoboride crystals may, in fact, be addressed as single crystalline foils rather than particles, since they possess a thickness of some unit cells yet have a lateral extension depending on the size of the host crystals, i.e. 10–100 μm. Spinodal decomposition is initiated by segregation of W. These W-rich areas are embedded in an unaffected, perfect AlB_2-structure type matrix and age to either W_2B_4 or β-WB, containing both some Ti and Cr, respectively.

Contamination from C and Co due to attrition milling with WC/Co milling balls, starting powder and the use of graphite lining has been discussed. Milling is necessary to decrease the grain size of the commercial raw materials and to provide a homogeneous phase distribution at the beginning of the hot-pressing cycle. Even though a processing route starting from the elements is principally possible, greater oxygen contamination and much higher costs would have to be tolerated. Moreover, it has been shown that the presence of C has beneficial effects regarding desoxidation. Although satisfactory densities with >97% of the theoretical value have been obtained, combustion routes or spark plasma hot-pressing could be advantageous.

A 40 mol% TiB_2, 50 mol% W_2B_4 and 10 mol% CrB_2 composition shows a microstructure with overall dispersed W_2B_4 precipitates most promising for *in situ* reinforcement. This system reaches its homogeneity range at around 2100 °C and forms two kinds of $(Ti,W,Cr)B_2$ solid solutions as a matrix. It decomposes into $(W,Cr,Ti)_2B_4$ and β-(W,Cr,Ti)B by annealing at lower temperatures, preferentially at 1650 °C for 4 h. The positive role of CrB_2 is clearly attributed to its high volume diffusion coefficient allowing for a rapid formation of solid solutions as well as a fast phase separation. Additionally, it stabilizes the β-(W,Cr,Ti)B phase which is considered to significantly improve fracture toughness.

Acknowledgements

The authors gratefully acknowledge the valuable contributions by the operators of the transmission electron microscopes B. Cappi, Institut für Gesteinshüttenkunde, F. Dorn, Gemeinschaftslabor für Elektronenmikroskopie, both RWTH Aachen University, and B. Freitag, Institut für Anorganische Chemie, University of Bonn. Microprobe analysis was carried out by W. Volkwein, HDZ GmbR, Würselen. The project was partially supported by the Deutsche Forschungsgemeinschaft (German Research Association, DFG) under the title "Nanostructured hard materials coatings in the $(Ti_xW_yCr_z)B_2$ system", Grant No Te146/27-1, which is gratefully acknowledged.

References

1. Sørlie M, Øye HA. Cathodes in aluminium electrolysis. 2nd ed. Düsseldorf: Aluminium-Verlag; 1994.
2. Bannister MK, Swain MV. A preliminary investigation of the corrosion of a TiB_2/BN/AlN composite during aluminium evaporation. *Ceram Int* 1989;**15**:375–82.
3. Becher PF, Rose LRF. Toughening mechanisms in ceramic systems. In: Cahn RW, Haasen P, Kramer EJ, editors. *Materials science and technology*, 11. Weinheim: Verlag Chemie; 1994. p. 409–62.
4. Telle R, Fendler E, Petzow G. The quasi-binary systems CrB_2–TiB_2, CrB_2–WB_2 and TiB_2–WB_2. *J Hard Mater* 1992;**3**:211–24.
5. Mader W, Freitag B, Kelm K, Telle R, Schmalzried C. Combined HRTEM and EFTEM study of precipitates in tungsten and chromium-containing TiB_2. In: *Mat. Res. Symp. Proc.; Mat. Res. Soc., 589*. 2001. p. 289–94.
6. Schmalzried C, Telle R, Freitag B, Mader M. Solid state reactions in transition metal diboride-based materials. *Z Metallkunde* 2001;**92**:1197–202.
7. Faber KT, Evans AG. Crack deflection processes – I. *Theory Acta Metall* 1983;**31**:565–76.
8. Kaga H, Carrillo-Heian EM, Munir ZA, Schmalzried C, Telle R. Synthesis of hard materials by field activation: the synthesis of solid solutions

and compositions in the TiB_2–WB_2–CrB_2 System. *J Am Ceram Soc* 2001;**84**:2764–70.
9. Lundström T. The structure of Ru_2B_3 and $WB_{2.0}$ as determined by single-crystal diffractometry, and some notes on the W-B-system. *Arkiv för Kemi* 1968;**30**:115–27.
10. Okada S, Takahashi Y, Higashi I, Atoda T. Preparation of single crystals of MoB_2 by the aluminium-flux technique and some of their properties. *J Mater Sci* 1987;**22**:2993–9.
11. Otani Sh, Ohashi H, Ishizawa Yo. Lattice constants and non-stoichiometry of WB_{2-x}. *J Alloys Compd* 1995;**221**:L8–10.
12. Woods HP, Wavner Jr FE, Fox BG. Tungsten diboride, preparation and structure. *Science* 1966;**75**:151.
13. Frotscher M, Klein W, Bauer J, Fang CM, Halet JF, Senyshin A, et al. M_2B_5 or M_2B_4? A reinvestigation of the Mo/B and the W/B system. *Z Allg Anorg Chemie* 2007;**633**:2626–30.
14. Mitra I, Telle R. Phase formation during anneal of supersaturated TiB_2–CrB_2–WB_2 solid solutions. *J Solid State Chem* 1997;**133**:25–30.
15. Fendler E, Babushkin O, Lindbäck T, Telle R, Petzow G. Modification of thermal mismatch in B_4C–diboride ceramics. *J Hard Mater* 1993;**4**:137–48.
16. Kuzenkova MA, Kayuk VG, Kislyi PS. Sintering of technical tungsten boride produced by the boron carbide process. *Sov Powder Metall Met Ceram* 1977;**16**:184–7.
17. Dushanek H, Rogl R. Critical assessment and thermodynamic calculation of the binary system Boron–Tungsten (B–W). *J Phase Equilibria* 1995;**16**:150–61.
18. Rogl P. Boron–carbon–tungsten. *Landolt-Börnstein, New Series IV/11E1*, vol. 24. Heidelberg: Springer; 2009. p. 1–30.
19. Wittmann A, Nowotny H, Boller H. Ein Beitrag zum Dreistoff Titan-Molybdän-Bor. *Monatshefte für Chemie* 1960;**4**:608–15.
20. Schmidt H, Borchardt G, Schmalzried C, Telle R, Baumann H, Weber S, et al. Material transport in $(Ti_{0.3}W_{0.5}Cr_{0.2})B_2$ ceramics: simultaneous diffusion of ion implanted ^{49}Ti and ^{54}Cr. *J Eur Ceram Soc* 2003;**23**: 991–5.
21. Aronson B, Lundström T, Engström I. Some aspects of the crystal chemistry of borides, boro-carbides and silicides of the transition metals. In: Vahldiek FW, Mersol SA, editors. *Anisotropy in single crystal refractory compounds*. New York: Plenum Press; 1968. p. 13–22.
22. Sigl LS, Kleebe HJ. Microcracking in TiB_2–B_4C composites. *J Am Ceram Soc* 1995;**78**:2374–80.
23. Telle R. Ceramics for high-tech applications. Material science, European concerted action COST 503 powder metallurgy – powder based materials. In: Valente T, editor. *Directorate-general, science, research and development*, vol. V. Brussels: European Community; 1997.
24. Sibuya M, Yoneda T, Yamamoto Y, Ohyanagi M, Munir ZA. Effect of Ni and Co additives on phase decomposition in TiB_2–WB_2 solid solutions formed by induction field activated combustion synthesis. *J Am Ceram Soc* 2003;**86**:354–6.
25. Sibuya M, Ohyanagi M. Effect of nickel additive on simultaneous densification and phase decomposition in TiB_2–WB_2 solid solutions by pressureless sintering using induction heating. *J Eur Ceram Soc* 2007;**27**:301–6.